



Disentangling the record of diagenesis, local redox conditions, and global seawater chemistry during the latest Ordovician glaciation



Anne-Sofie C. Ahm^{a,*}, Christian J. Bjerrum^a, Emma U. Hammarlund^b

^a Nordic Center for Earth Evolution, Department of Geoscience and Natural Resource Management, University of Copenhagen, Øster Voldgade 10, DK-1350 Copenhagen K, Denmark

^b Nordic Center for Earth Evolution, Department of Biology, University of Southern Denmark, DK-5230 Odense C, Denmark

ARTICLE INFO

Article history:

Received 8 March 2016

Received in revised form 26 September 2016

Accepted 27 September 2016

Available online 24 October 2016

Editor: D. Vance

Keywords:

glacioeustasy

deep water anoxia

Hirnantian extinction

multivariate statistics

iron speciation

sulfur isotopes

ABSTRACT

The Late Ordovician stratigraphic record integrates glacio-eustatic processes, water-column redox conditions and carbon cycle dynamics. This complex stratigraphic record, however, is dominated by deposits from epeiric seas that are susceptible to local physical and chemical processes decoupled from the open ocean. This study contributes a unique deep water basinal perspective to the Late Ordovician (Hirnantian) glacial record and the perturbations in seawater chemistry that may have contributed to the Hirnantian mass extinction event. We analyze recently drilled cores and outcrop samples from the upper Vinini Formation in central Nevada and report combined trace- and major element geochemistry, Fe speciation ($\text{Fe}_{\text{Py}}/\text{Fe}_{\text{HR}}$ and $\text{Fe}_{\text{HR}}/\text{Fe}_{\text{T}}$), and stable isotope chemostratigraphy ($\delta^{13}\text{C}_{\text{Org}}$ and $\delta^{34}\text{S}_{\text{Py}}$). Measurements of paired samples from outcrop and core reveal that reactive Fe is preserved mainly as pyrite in core samples, while outcrop samples have been significantly altered as pyrite has been oxidized and remobilized by modern weathering processes. Fe speciation in the more pristine core samples indicates persistent deep water anoxia, at least locally through the Late Ordovician, in contrast to the prevailing interpretation of increased Hirnantian water column oxygenation in shallower environments. Deep water redox conditions were likely decoupled from shallower environments by a basinal shift in organic matter export driven by decreasing rates of organic matter degradation and decreasing shelf areas. The variable magnitude in the record of the Hirnantian carbon isotope excursion may be explained by this increased storage of isotopically light carbon in the deep ocean which, in combination with increased glacio-eustatic restriction, would strengthen lateral- and vertical gradients in seawater chemistry. We adopt multivariate statistical methods to deconstruct the spatial and temporal re-organization of seawater chemistry during the Hirnantian glaciation and attempt to isolate the latent magnitude and global perturbation in the carbon cycle. We speculate, using a two component mixing model and residual estimates from principal component analysis, that the secular open ocean Hirnantian C isotope excursion possibly amounts to only $\sim +1.5\%$. Such an increase could be mechanistically driven by the combination of sea-level fall, persistent deep water anoxia, and cooler glacial temperatures that increased the organic carbon burial efficiency in the deeper basins.

© 2016 Elsevier B.V. All rights reserved.

1. Introduction

The ice-house conditions of the Hirnantian (latest Ordovician ~ 444 Ma) coincide with the first of five major Phanerozoic mass extinctions (Berry and Boucot, 1973; Raup and Sepkoski, 1982). The concomitance of the mass extinction event and glaciation has been used to argue a causal relationship associated with a perturbation in the global carbon cycle recorded by a positive

excursion in stable C isotopes of both carbonates and organic matter ($\delta^{13}\text{C}_{\text{Carb}}$ and $\delta^{13}\text{C}_{\text{Org}}$, respectively, Brenchley et al., 1994; Melchin et al., 2013). However, the specific glacio-eustatic process that could cause a major Hirnantian carbon isotope excursion and mass extinction remain ambiguous. Previous studies propose a number of plausible drivers, such as increased thermohaline circulation and marine productivity during the glacial interval, increased limestone weathering from carbonate platforms exposed by the glacio-eustatic sea-level fall, and increased silicate and phosphorus weathering driven by the colonization of the first land plants (Brenchley et al., 1994; Kump et al., 1999; Lenton et al., 2012).

* Corresponding author.

E-mail address: ascahm@gmail.com (A.-S.C. Ahm).

The discrepancies surrounding the Hirnantian carbon cycle partly originate from intricate glacial ocean dynamics and re-organization of water column redox conditions such as those observed more recently during the Pleistocene glaciations. Cooler glacial temperatures during the Hirnantian would likely have increased oxygen saturation in surface seawater, in particular at high latitudes where deep- and intermediate water masses are presently sourced (e.g. Jaccard and Galbraith, 2012). However, water column oxygen is intimately tied to the carbon cycle and controlled by the export and degradation of organic matter (Southam and Hay, 1977). Glacio-eustatic processes are noted to transfer the export of organic carbon and oxygen demand towards the open ocean (Cartapanis et al., 2016; Jaccard et al., 2009). These processes involve changes in ocean circulation, decreasing metabolic rates of organic matter degradation associated with cooler temperatures, and decreasing shelf area (Bjerrum et al., 2006; Finnegan et al., 2012). In the Pleistocene, for example, these mechanisms are observed to result in diminishing Oxygen Minimum Zones (OMZs) on the outer shelf and decreasing oxygen concentrations in the deep ocean (Cartapanis et al., 2016; Jaccard et al., 2009). The Hirnantian stratigraphy potentially records similar changes of locally increased oxygenation in shallow water environments while widespread anoxia developed in deeper basins (Hammarlund et al., 2012). The Hirnantian stratigraphic record, however, is dominated by deposits from epeiric seas that are susceptible to local processes that are decoupled from the open ocean (e.g. Jones et al., 2011, in press). An understanding of spatial variability in seawater chemistry is thus essential to reconstruct the secular record of Hirnantian redox conditions and carbon-cycle dynamics.

Extensive Hirnantian sedimentary rocks in central Nevada offer a unique context to investigate the past environmental conditions across a transect from shelf to basin during the glaciation. Deep water facies are rarely preserved in the ancient geological record due to the continuous subduction of the ocean floor. In Nevada, however, Hirnantian deep water siliciclastic facies of the Roberts Mountain thrust plate have been juxtaposed with coeval shallow carbonate ramps following the late Devonian Antler orogeny (Merriam and Anderson, 1942; Finney et al., 2000). This study contributes analyses of outcrop samples and new shallow drill core samples from the deep basinal Vinini Formation (Fm.) of Roberts Mountain. We report combined major- and trace element geochemistry, Fe speciation, and stable isotope chemostratigraphy ($\delta^{13}\text{C}_{\text{Org}}$ and $\delta^{34}\text{S}_{\text{Py}}$). A Monte Carlo approach is used to quantify the propagation of uncertainty in Fe speciation measurements and evaluate the effects of modern oxidative weathering on the speciation of Fe-rich phases. Multivariate statistical methods are adopted to deconstruct the spatial and temporal re-organization of sea water chemistry and redox conditions during the Hirnantian glaciation, and used to isolate the latent magnitude and global perturbation in the carbon cycle.

2. Geological setting

Late-Ordovician strata are exposed in the upper 30 m of the Vinini Formation in the Roberts Mountain (Fig. S1). In 1994, Finney et al. (1998) excavated the Vinini Creek section by bulldozer and exposed a unique deep-marine Late-Ordovician section recording the Hirnantian glacial interval. The excavated Vinini Creek section has since been thoroughly studied (e.g. Finney et al., 1998, 1999, 2007; LaPorte et al., 2009; Rohrssen et al., 2013).

The Vinini Creek section spans from the mid Katian to the lowest Silurian and has been correlated to other Ordovician sections based on graptolite biostratigraphy (Fig. 1) (Finney et al., 1999). The bottom of the section (0–9.8 m) covers the upper part of the Katian *D. ornatus* biozone (~447.87–446.20 Ma) and consists of interbedded siltstone and periplatform limestone mud deposited by

density currents in lower slope to basin-margin settings (Finney et al., 2007). The overlying 9.8–17.0 m strata cover the upper Katian *P. pacificus* biozone (~446.20–444.68 Ma) consisting of organic-rich interbedded black shale and siliceous ooze. Previously, this specific interval has been interpreted as reflecting a development of an OMZ in overlying waters on the outer shelf during sea-level highstand (Finney et al., 1999, 2007; LaPorte et al., 2009). The transition to the Hirnantian glacial stage is marked by a pronounced change from siliciclastic dominated sediments in the upper Katian to carbonate dominated sediment in the Hirnantian. However, the Hirnantian transition is complicated by a tectonic fault underlying the Hirnantian *M. extraordinarius* biozone (Fig. 1A). This structural feature potentially marks a smaller unconformity and may additionally be prone to post-depositional fluid flow along the fracture zone. Above this zone, the *M. extraordinarius* biozone (~444.68–444.13 Ma) contains both the first extinction pulse and the glacial maximum. This interval is characterized by tan-gray periplatform dolomites and transitions into micritic limestone in the *M. persculptus* biozone (~444.68–443.41 Ma). The lithological transition has been linked to ice house dynamics and a possible interglacial period in the mid Hirnantian (Melchin et al., 2013). The transition from the Hirnantian- to the Silurian is marked by a shift to distinct green shale across an unconformity, where the top of the *M. persculptus* biozone and much of the lower Llandovery (lower Silurian) is missing.

3. Methods

In the fall of 2012 and 2013, we collected outcrop and core samples throughout the Vinini Creek section. Outcrop samples were recovered every ~10 cm from the bulldozed trench using a hammer and chisel after removing the top layer of obviously weathered rock. In addition, we obtained multiple shallow drill-cores through specific intervals. The boreholes were drilled near vertically at an oblique angle to the dipping beds covering a total of ~12.7 m of the total 26 m of measured outcrop. The cores were obtained using a hand held portable rock drill with a 41 mm diamond core bit mounted on a 122 cm long threaded lead with a water circulation system (Tanka engine drill re-gearred from Shaw Tool's). Extension core barrels were used, permitting a total vertical drill depth of up to 10 m under ideal conditions (Bjerrum, unpublished). Core and outcrop samples were correlated to within decimeter scale precision by both drilling depth and sedimentology and further related to previous published data by litho- and organic carbon isotope stratigraphy (Fig. 1). All comparisons between core- and outcrop samples are restricted to the top 15 m of the section and exclude the lower Katian stratigraphy where no cores have been drilled.

All samples comprise ~1–2 cm³ of rock that were freeze dried before storage and subsequently split, crushed and homogenized to powder <125 μm . A tungsten-carbide shatterbox was used to crush core samples while outcrop samples were drilled using a coated Ti–Al hardened steel drill for selective sampling to avoid impurities such as veins and clearly weathered rock.

3.1. Geochemical analysis

The majority of carbon measurements were performed at the University of Copenhagen and a subset of samples were measured at Iso-Analytical Limited (UK) using similar methods. Carbonate content was approximated by mass loss following acid treatment in 10% HCl heated to 80 °C for 1 h. Total Organic Carbon (TOC) was measured on the basis of CO₂ (g) released from the decarbonized material during combustion using a Metalyt CS-500 and reported as a percentages of the total mass of the original sample. Long-term reproducibility of the instrument is better than $\pm 0.2\%$

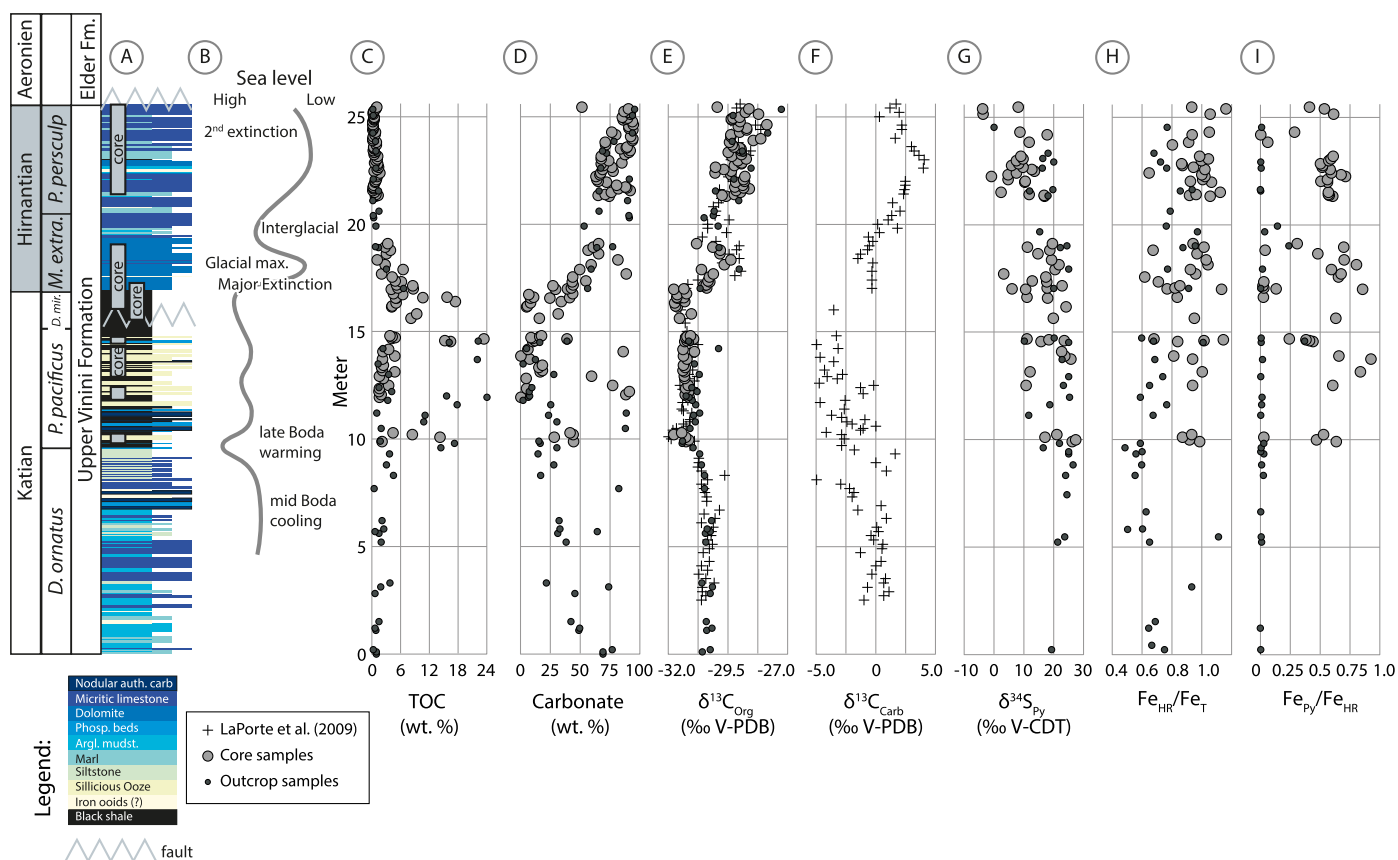


Fig. 1. Stratigraphy of the Hirnantian Vinini Creek section. **A.** Lithostratigraphic column colored by facies and correlated with previous published graptolite biozones (Finney et al., 1999; LaPorte et al., 2009; Melchin et al., 2013). The length of the *D. mirus* Subzone is approximated by correlation with LaPorte et al. (2009), but is uncertain due to faulting across this interval. **B.** Interpreted sea-level curve during the Late Ordovician (modified from Ghienne et al., 2014; Holmden et al., 2013; Sheets et al., 2016). **C.** Stratigraphic variations in the concentration of Total Organic Matter (TOC). **D.** Variations in carbonate content. **E.** Variations in $\delta^{13}\text{C}_{\text{Org}}$ recording the Hirnantian carbon isotope excursion in agreement with previous measurements of both $\delta^{13}\text{C}_{\text{Org}}$ and $\delta^{13}\text{C}_{\text{Carb}}$ (from LaPorte et al., 2009). **G.** $\delta^{34}\text{S}_{\text{Py}}$ showing a broadly negative trend up section. **H.** Variations in $\text{Fe}_{\text{HR}}/\text{Fe}_{\text{T}}$ (diagnostic anoxic threshold ~ 0.38) and **I.** variations in $\text{Fe}_{\text{Py}}/\text{Fe}_{\text{HR}}$ with diagnostic euxinic threshold ~ 0.8 , indicating persistent anoxia during the latest Ordovician (Poulton and Canfield, 2011).

for TOC and $\pm 0.3\%$ for TS. Organic carbon isotope composition ($\delta^{13}\text{C}_{\text{Org}}$ ‰ V-PDB) was measured on the decarbonized sediment and determined with a Thermo Analytical Elemental Analyser coupled to a Micromass IsoPrime isotope ratio mass spectrometer with a precision of $< 0.2\%$.

Paleo-redox conditions were explored using sequential iron extraction techniques. These analyzes were performed according to the methods of Poulton and Canfield (2005) that partitions iron into its highly reactive components and its unreactive phases. Highly reactive iron (Fe_{HR}) represents the non-silicate bound iron that is geochemically and biologically active during early sediment diagenesis (Poulton and Canfield, 2011). Fe_{HR} includes iron oxide (Fe_{Ox}), carbonate iron minerals such as siderite (Fe_{Carb}), iron in magnetite (Fe_{Mag}), and pyrite (Fe_{Py}). The concentrations of the iron species (Fe wt.%) obtained from the chemical extraction were quantified by Atomic Adsorption Spectroscopy (AAS) with a long-term reproducibility of the complete extraction procedure of $\pm 0.166\%$ (2σ , $n = 31$). Total Fe (Fe_{T}) was measured using an Olympic DP-6000 handheld XRF as detailed below. The combined wet extraction and XRF measurements yield a $\text{Fe}_{\text{HR}}/\text{Fe}_{\text{T}}$ precision that is proportional to the statistical uncertainty of the independent measurements of Fe_{HR} and Fe_{T} (Fig. S3). We use a Monte Carlo algorithm to calculate the error propagation by re-sampling both Fe_{HR} and Fe_{T} ten-thousand times within the uncertainty range. We find that the 2σ confidence level (95%) increases with lower concentrations of iron (Fig. S3). Five samples have ambiguous ratios above 1 that cannot be explained by the statistical uncertainty and are excluded from further analysis. One possible

explanation for these outliers could be the presence of acid volatile sulphides, which contribute to overestimation of Fe_{HR} (Poulton and Canfield, 2005). Based on the Monte Carlo analysis all samples with $\text{Fe}_{\text{T}} < 0.5\%$ are excluded from further analysis. A similar minimum Fe_{T} requirement of $< 0.5\%$ has previously been established in carbonate-rich rocks (Clarkson et al., 2014).

Total Sulfur (TS) measurements were included in the measurements of the decarbonized material on the Metalyt CS-500 at the University of Copenhagen and likewise corrected for carbonate loss. Pyrite sulfur (Fe_{Py}) was measured at the University of Southern Denmark based on chromium reduction, trapped as Ag_2S , followed by gravimetric determination of pyrite concentration (Canfield et al., 1986). Acid volatile sulphides were not extracted separately in this study as this component is expected to represent a minor sulphide phases in ancient sedimentary rocks. An analysis of the potential impact of AVS on our results is presented in the supplementary information.

The sulfur isotopic composition of pyrite ($\delta^{34}\text{S}_{\text{Py}}$) was determined using a Thermo Analytical Elemental Analyser, Flash EA 1112 series coupled via a ConFlo IV interface to a Thermo Delta V Plus mass spectrometer. Isotope data are reported in terms of permil relative to the Vienna Canyon Diablo Troilite (V-CDT), with a precision of $< 0.3\%$.

Major- and minor elements were determined from the powdered rock samples following methods outlined by Dahl et al. (2013) using an Olympic DP-6000 handheld XRF analyzer (HH-XRF) with a Rh tube at 40 and 10 kV. The average relative external precision across all reported elements is 12.9% (Fig. S2). Addition-

ally, a subset of samples and a range of in-house and international standards were measured by Inductively Coupled Plasma Mass spectrometry (ICP-MS) for calibration of HH-XRF measurements based on a reduced major axis linear regression model (Table S1 and Fig. S2). Specifically with regard to the Fe speciation, the R^2 correlation coefficient between HH-XRF and ICP measurements of total Fe is >0.99 . Trace element ICP analysis were performed at the Geological Survey of Denmark and Greenland, where 100 mg rock powder was digested in a mixture of hydrofluoric and nitric acid in closed Teflon vessels on a hotplate at 130°C for a minimum of 24 h. Drying and re-dissolving was performed as above, before an internal standard solution and Milli-Q water was added. The vessels were closed and placed on the hotplate at 130°C for a minimum of 12 h and then diluted to 50 mL. Trace element content was measured using a PerkinElmer Elan 6100DRC ICP-MS with an accuracy of better than 11% for USGS certified basalt reference (BHVO-2).

3.2. Multivariate statistical analysis

The multivariate geochemical dataset from the Vinini Creek section holds clues to past local and global environmental changes, early diagenetic processes, and post-depositional alterations. These combined signals may be disentangled by isolating specific geochemical trends that are expressed across a range of variables. This kind of geochemical redundancy can be harnessed to reduce the dimensionality of the dataset. Detailed inspection of the groups of variables that respond in concert provides the opportunity to extract the dominant processes that are recorded in the physical and chemical stratigraphy (see supplementary material).

Distinct geochemical trends in a multivariate dataset may be identified by Principal Component Analysis (PCA) (Hammer and Harper, 2006). These trends are recast as principal components, constructed by orthogonal linear combinations of the original geochemical variables, ordered based on their contribution to the total variability of the dataset (Hammer and Harper, 2006; Marden, 2015). In practice, the analysis uses the covariance matrix of the dataset to calculate the eigenvectors and eigenvalues for each geochemical variable, where the eigenvalues represent the order of significance for each component (see supplementary information, Marden, 2015). In extension to PCA, Factor Analysis (FA) is used to remove less significant components from the dataset (Hammer and Harper, 2006). This method isolates a few geochemical trends responsible for a larger part of the variance in the multivariate dataset. The trends are isolated by fitting a preassigned number of common factors (vectors) to the dataset and represented in a multidimensional coordinate system (Marden, 2015). We can use these combined statistical methods to identify principal components that may be interpreted as reflecting underlying geochemical processes with environmental significance. Furthermore, the residual unexplained variance may be used to detect latent less significant trends in the geochemical expression. The reduced dataset is from here on referred to as the reduced PCA model (see supplementary information).

In combination with PCA and FA, cluster analysis may illustrate the finer detailed relationship within characteristic groups (clusters) of variables that respond in concert (Hammer and Harper, 2006). Clusters are computed using the non-parametric Spearman distance, and variables are hierarchically ordered by links into binary clusters using an average linkage clustering algorithm (Hammer and Harper, 2006). These clusters are illustrated in a dendrogram, where the correlation between geochemical variables is characterized by their standardized distance as represented by the length of each “branch”. The specific clustering of geochemical elements may reveal details of the higher-order relationships among variables within the larger PCA and FA based groupings,

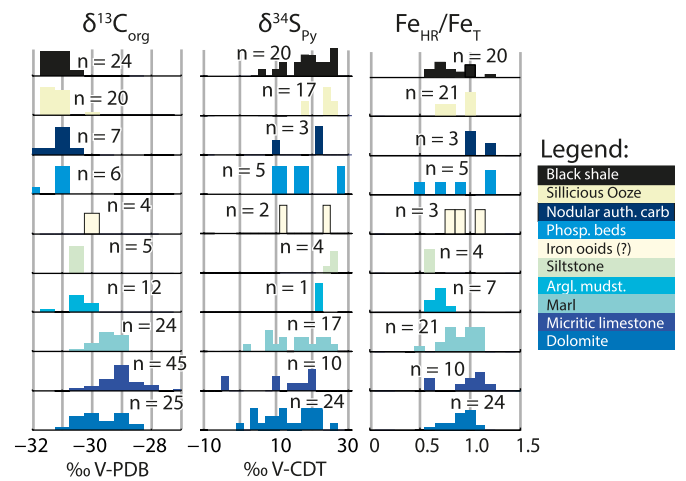


Fig. 2. Histograms of geochemical variation of $\delta^{13}\text{C}_{\text{org}}$, $\delta^{34}\text{S}_{\text{py}}$, and $\text{Fe}_{\text{HR}}/\text{Fe}_{\text{T}}$ with facies distribution. In contrast to $\delta^{34}\text{S}_{\text{py}}$ and $\text{Fe}_{\text{HR}}/\text{Fe}_{\text{T}}$, the histogram of $\delta^{13}\text{C}_{\text{org}}$ illustrates a behavior that visually follows the distribution of facies.

which may be used to identify the underlying geochemical processes.

4. Results

4.1. Chemostratigraphy

The Hirnantian carbon isotope excursion is recorded in the upper Vinini Fm. (Fig. 1) (Finney et al., 1999; LaPorte et al., 2009). Variations in $\delta^{13}\text{C}_{\text{org}}$ appear to visually coincide with distinct sedimentological facies that reflect the late Ordovician glacio-eustatic evolution (Fig. 2): the lower slope setting of the *D. Ornatu*s biozone has baseline $\delta^{13}\text{C}_{\text{org}}$ values of $\sim -30.5\%$. The overlying *P. Pacificus* biozone is dominated by black shales with a small -1% $\delta^{13}\text{C}_{\text{org}}$ excursion that has been interpreted to coincide with the late Katian sea-level highstand (Finney et al., 2007; LaPorte et al., 2009; Melchin et al., 2013). The overlying glacial interval is dominated by carbonate deposits and records a positive $\sim +2-3\%$ increase in $\delta^{13}\text{C}_{\text{org}}$ that has been identified as the Hirnantian carbon isotope excursion (Finney et al., 1999; LaPorte et al., 2009). This interval is superimposed by a short-lived $\sim -1\%$ excursion that may correlate with a brief mid Hirnantian interglacial (Melchin et al., 2013).

This study only reports $\delta^{13}\text{C}_{\text{org}}$ measurements but for comparison previous published $\delta^{13}\text{C}_{\text{carb}}$ measurements from the Vinini Creek section has been included in Fig. 1 (LaPorte et al., 2009). Similarly to $\delta^{13}\text{C}_{\text{org}}$, the Hirnantian carbon isotope excursion is recorded in $\delta^{13}\text{C}_{\text{carb}}$ by a $\sim +2-3\%$ increase. Measurements from the upper Katian *P. Pacificus* biozone, however, have previously been determined to be influenced by diagenetic alteration, partly due to the very low concentrations of carbonate in this interval (Fig. 1) (LaPorte et al., 2009).

Measurements of $\delta^{13}\text{C}_{\text{org}}$ reveal a proportional relationship with the concentration of TOC, such that low values of $\delta^{13}\text{C}_{\text{org}}$ correlate with high concentrations of TOC and vice versa (Fig. 3). The non-linear correlation between $\delta^{13}\text{C}_{\text{org}}$ and TOC can be simulated using a simple two component mixing model where two distinct sediment sources with different concentrations of TOC and different $\delta^{13}\text{C}_{\text{org}}$ values are proportionally mixed (Johnston et al., 2012). Samples from the Hirnantian part of the section are better approximated by the mixing model ($R^2 = 0.46$) than Katian samples ($R^2 = 0.22$) (Fig. 3).

A positive excursion in sulfur pyrite isotopes ($\delta^{34}\text{S}_{\text{py}}$) is widely observed in parallel with the Hirnantian carbon isotope excursion (Hammarlund et al., 2012; Jones and Fike, 2013). However, this canonical trend is not expressed in the measured $\delta^{34}\text{S}_{\text{py}}$ from

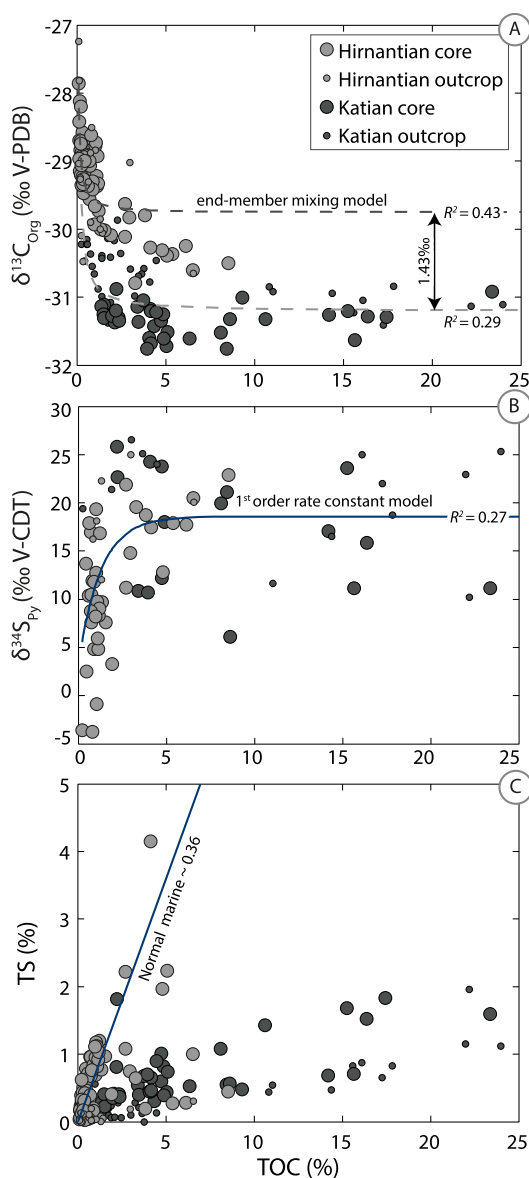


Fig. 3. $\delta^{13}\text{C}_{\text{Org}}$, $\delta^{34}\text{S}_{\text{Py}}$, and TS demonstrate highly non-linear relationships with TOC. **A.** $\delta^{13}\text{C}_{\text{Org}}$ versus TOC can be simulated by simple end-member mixing models involving different end-members in the Katian samples (end-member 1 having TOC $\sim 0.7\%$ and $\delta^{13}\text{C}_{\text{Org}} \sim -30.64\%$ and end-member 2 having TOC 26% and $\delta^{13}\text{C}_{\text{Org}} \sim -31.19\%$) and Hirnantian samples (end-member 1 having TOC $\sim 0.1\%$ and $\delta^{13}\text{C}_{\text{Org}} \sim -27.51\%$ and end-member 2 having TOC $\sim 20\%$ and $\delta^{13}\text{C}_{\text{Org}} \sim -29.76\%$). **B.** $\delta^{34}\text{S}_{\text{Py}}$ versus TOC can be estimated by a 1st order exponential kinetic rate model comparable to laboratory experiments of sulfate reduction rates in terms of labile organic matter (Leavitt et al., 2013; Sim et al., 2011). **C.** Cross plot of TS against TOC indicates a significant difference between the Katian and Hirnantian compared to normal marine ratios (~ 0.36 ; Morse and Berner, 1995; Raiswell and Canfield, 2012).

the Vinini Creek section. Rather, our measurements reveal generally enriched $\delta^{34}\text{S}_{\text{Py}}$ values ($\sim +20\%$) that weakly anti-correlate with $\delta^{13}\text{C}_{\text{Org}}$ and TOC and show a broad negative trend up section (Fig. 1). The observed non-linear correlation between TOC and $\delta^{34}\text{S}_{\text{Py}}$ can be simulated using an exponential model with an $R^2 = 0.27$. The concentration of TOC, furthermore, correlates with the absolute concentration of sulfur (TS) in a linear fashion, but with a distinctly different slope for Katian and Hirnantian samples (0.79 and 0.16, respectively, Fig. 3C).

Past redox conditions can be characterized by the speciation of Fe, with anoxic enrichment of Fe_{HR} identified by ratios of $\text{Fe}_{\text{HR}}/\text{Fe}_{\text{T}}$ above 0.38 (Poulton and Canfield, 2011). This threshold is cali-

brated against modern sediments and reflects the anoxic enrichment of authigenic Fe mineral phases in both carbonates and siliciclastics (Clarkson et al., 2014; Poulton and Canfield, 2011). The calculated confidence intervals show that all but two samples from the Vinini Creek section are, within 95% confidence, above the diagnostic anoxic threshold (Fig. 1). Fe speciation was measured in both samples from outcrop and shallow cores drilled on site (Finney et al., 1998). These measurements demonstrate an excess of Fe oxides in outcrop samples compared to core samples, and significant differences in the ratio of pyrite ($\text{Fe}_{\text{Py}}/\text{Fe}_{\text{HR}}$) between core and outcrop samples (~ 0.7 to 0.0 , respectively) (Fig. 4). Furthermore, $\text{Fe}_{\text{HR}}/\text{Fe}_{\text{T}}$ is depleted by up to $\sim 30\%$ in outcrop samples compared to core samples. The differences in Fe chemistry between core and outcrop increase down core along a decimeter thick profile (core-top samples; Fig. 4). The difference between core and outcrop samples is also expressed in $\delta^{34}\text{S}_{\text{Py}}$. Outcrop samples are slightly enriched compared to the core, above the natural scatter of the measurements (Fig. 4). In contrast, there seem to be no apparent difference between core and outcrop for the remaining measured proxies.

4.2. Multivariate analysis and trace element geochemistry

The Late Ordovician stratigraphy reflects many complex intertwined processes such as past biogeochemical cycling, early diagenetic sedimentary processes, and post depositional alterations. XRF measurements of major- and minor elements can provide clues to the interpretation of the sedimentary record across a range of properties. These measurements thus increase the redundancy in the combined dataset which result in grouping of specific elements that potentially tracks individual processes. We use multivariate statistical models (PCA and FA, see methods) to explore the geochemical dataset and harness patterns that may identify the governing mechanisms.

PCA is used to group elements into principal components based on their covariance. The analysis demonstrates that the first principal component explains more than 35% of the variance in the entire dataset and that three principal components explain 65% of the variance (Fig. 5). These results imply a large redundancy across the geochemical measurements that may track only a few specific depositional processes.

FA is used to reduce the dimensionality of the dataset by limiting the analysis to the first three principal components or common factors, thereby excluding much of the geochemical noise (Fig. 5). With factor analysis, we can explore how different elements vary within each component, and use our geological knowledge to identify the governing processes. The first component in the factor analysis model is associated with elements that are often related to detrital input, such as Al, K, Zr, Rb and Ti (Wedepohl, 1971). In parallel, elements that are often associated with organic matter (TOC), such as Cu, Ni, V, and Zn demonstrate a strong covariance within the second component (Tribovillard et al., 2006). This component also correlates with the redox sensitive elements Mo and U. The third component of the model reveals covariance between carbonate content, Sr and Mn. Also, $\delta^{13}\text{C}_{\text{Org}}$ has the highest loadings in this third carbonate-dominated component, which in part substantiates the observed correlation with facies for $\delta^{13}\text{C}_{\text{Org}}$ (Fig. 5). Iron speciation, $\delta^{34}\text{S}_{\text{Py}}$, and total S, on the other hand, show little covariation with any of the components from the common factor model (Fig. 5).

The redundancy and grouping of the dataset can be further explored by hierarchical cluster analysis. The specific clustering of elements reveals details of the higher-order relationships within each component. These relationships are illustrated in a classical dendrogram, where the length of each branch reflects the similarity between variables. For example, Al, K, and Rb demonstrate

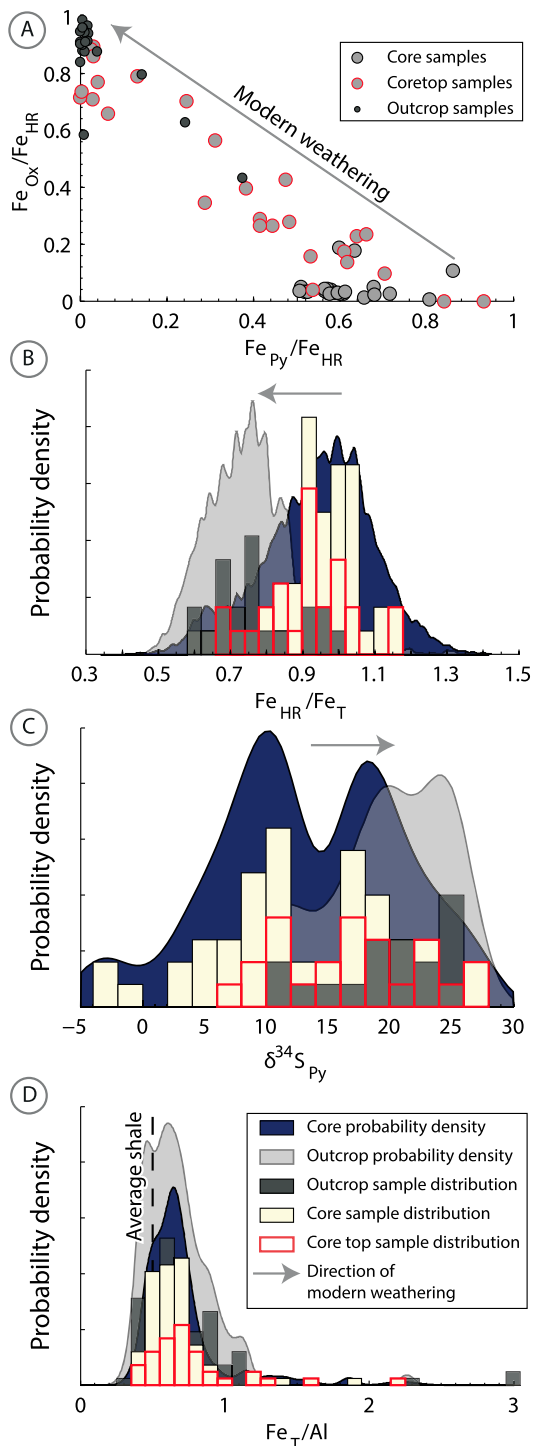


Fig. 4. Comparison of the Fe speciation proxy between outcrop and core samples revealing significant alteration due to modern oxidative weathering (despite recent excavated outcrop exposure, Finney et al., 1998). Core and outcrop samples were correlated within decimeter scale precision by both drilling depth and sedimentology. Comparisons are restricted to the top 15 m of the section and exclude the lower Katian stratigraphy where no cores have been drilled. **A.** Cross plot illustrating the difference between pyrite (Fe_{Py}) and Fe-oxide (Fe_{Ox}) in core and outcrop samples, with core-top samples recording transient progressive alteration. **B.** Overlain histograms illustrating the difference in Fe_{HR} between core and outcrop samples. The probability density curve illustrates the propagation of uncertainty in the measurements, simulated using a Monte Carlo algorithm. **C.** Histogram illustrating the difference in $\delta^{34}S_{Py}$ between core and outcrop, with the probability density curve showing the Gaussian distribution. **D.** Total Fe relative to Al is enriched in both outcrop and core samples compared to average shale.

the strongest relationship in the dataset (shortest branch, Fig. 5C). The cluster analysis illustrates that the detrital, organic, and carbonate related components are grouped into three major clusters. Furthermore, there seem to be little relationship between Fe speciation, TS, and these major components. Limiting the analysis to core samples only does not change the major trends and groupings of the dataset (Fig. S6).

The grouping of specific elements into each component matches our general understanding of sedimentary ingredients: one component likely represents the detrital input, a second component represents the input of organic matter, and a third component may reflect carbonate input. We can test this hypothesis by modeling the trends in detrital components such as Al, organic matter (TOC), and $CaCO_3$ by using a three component reduced PCA model (see methods). The PCA reconstruction demonstrates that the reduced model to a large degree fits the observed trends for these elements, with little residual unexplained variability as expressed by the deviation from the 1:1 identity line ($R^2 = 0.87, 0.87, \text{ and } 0.84$, respectively, Fig. 6). We can further use the reduced PCA model to test the correlation between sedimentary mixing, as inferred from the three major components, and other measured elements. The unexplained residual components from the analysis may reveal distinct trends that demonstrate little covariance with sedimentary mixing and provide further insight into past environmental processes.

5. Discussion

The Late Ordovician stratigraphy integrates temporal glacio-eustatic changes with complex ocean redox and nutrient cycle dynamics. This record is complicated by both the spatial progradation of facies driven by sea-level fall and by further post-depositional secondary changes in the geochemical expression. We apply a multi-proxy approach to the deep water strata of the upper Vinini Fm. to deconstruct the complexity of integrated environmental and secondary signals.

5.1. Post-depositional diagenetic considerations

Fe speciation measurements from paired outcrop and core reveal that reactive Fe is continuously remobilized by modern weathering processes (Fig. 4). These mechanisms are in part captured in outcrop samples by the progressive alteration of pyrite minerals into Fe oxides. The result is a significant differences in Fe_{Py}/Fe_{HR} between core and outcrop samples (0.51 ± 0.25 vs. 0.04 ± 0.09 , respectively; Fig. 4A). Although these observations are in line with the general expectation of pyrite weathering, the rate and amount of pyrite loss is significant larger than previously assumed (Canfield et al., 2008). The modern alteration of pyrite has additionally contributed to a loss of total reactive Fe and depleted ratios of Fe_{HR}/Fe_T in outcrop compared to core samples (Fig. 4B). Such loss of Fe_{HR} is unexpected and has not previously been documented. The increased acidity produced by pyrite dissolution would contribute to increased solubility of reactive Fe. However, we observe no significant difference in Fe_T between outcrop and core possibly indicating that remobilized reactive Fe is incorporated into unreactive phases such as authigenic clay minerals (Fig. 4 and S4, Curtis et al., 1985). We speculate that the simultaneous weathering of pyrite, organic sediments, and carbonates, may cause large fluctuations in pH where more neutral values would favor precipitation of Fe-rich aluminosilicates (Curtis et al., 1985).

Modern weathering in outcrop clearly alters pyrite concentrations, which potentially may affect $\delta^{34}S_{Py}$. Laboratory experiments suggest that abiotic H_2S oxidation may result in up to $\sim 5\%$ enrichment of S isotopes in the sediment due to continuous faster

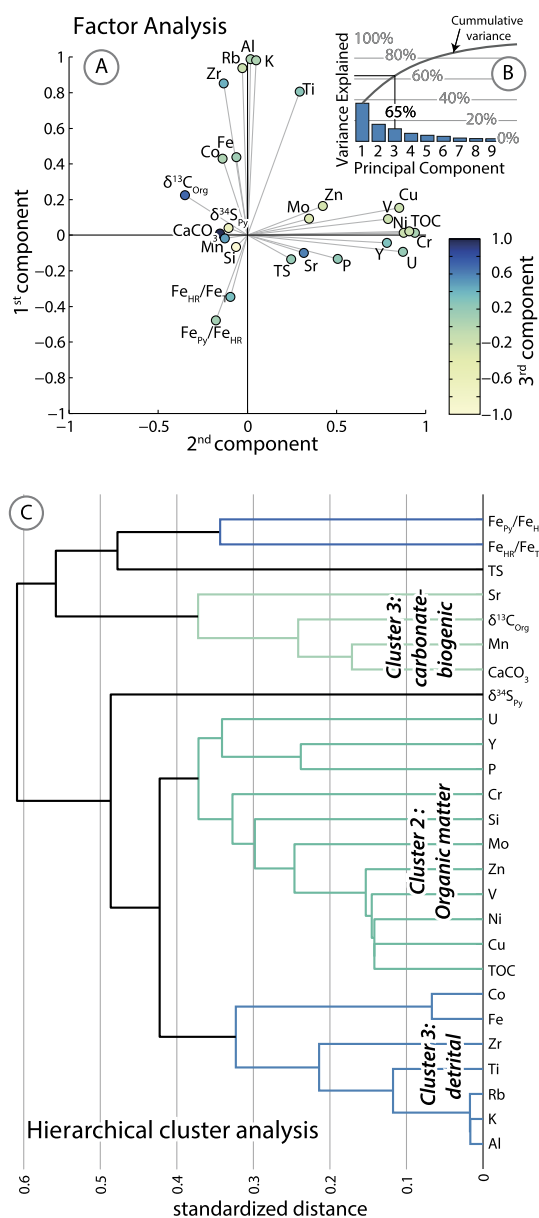


Fig. 5. Multivariate analysis exploring covariance between the 26 geochemical variables in the dataset. **A.** Factor analysis demonstrating the covariance between variables when modeled using three common factors. **B.** Number of principle components that explain the observed geochemical variance. **C.** Dendrogram illustrating the hierarchical clustering of variables where the length of each branch represents the spatial standardized distance. The cluster analysis reveals three dominant clusters, likely representing the detrital, organic matter, and carbonate sedimentary components.

remobilization of the lighter isotope (Fry et al., 1988). We observe seemingly similar enrichment in outcrop samples, but the large natural scatter and spread observed in $\delta^{34}\text{S}_{\text{Py}}$ may hide much of the additional isotopic enrichment due to modern weathering processes (Fig. 4C).

The combined Fe speciation and $\delta^{34}\text{S}_{\text{Py}}$ dataset indicate the potential magnitude and direction of change that surface weathering processes may cause in these proxies. Specifically, in our case, the location of the Vinini Creek section in the central Nevada high desert may contribute to the substantial extent of modern oxidative weathering. Previous studies of modern surface weathering in black shales have demonstrated significant loss of total organic carbon in addition to loss of trace elements, particularly Mn and elements associated with sulfides (Perkins and Mason, 2015;

Petsch et al., 2000). Despite the significant degree of surface weathering, these trends are not observed in the Vinini Formation, suggesting that these elements are quantitatively captured in oxides or other secondary mineral phases. The differences in Fe speciation and S isotopes between outcrop and core samples highlights the need for caution when attempting to catalog past environmental redox change from purely outcrop based records. In this study, we interpret the stratigraphic variation in Fe speciation and S isotope based purely on core samples.

$\text{Fe}_{\text{HR}}/\text{Fe}_{\text{T}}$ in core samples demonstrates constant enrichment above the diagnostic anoxic threshold throughout the Vinini Creek section (within 95% confidence interval; Fig. S3). Enrichment can, however, also occur during later stage diagenesis, where Fe in clay minerals and iron oxides may be re-mobilized and altered at high temperatures (Curtis et al., 1985). During this diagenetic process Fe^{3+} is eliminated from dioctahedral detrital clays and reduced to Fe^{2+} , which can be incorporated into authigenic trioctahedral clays or reactive non-silicate phases (Curtis et al., 1985). The Vinini Fm., as part of the Roberts Mountain allochthon, must have experienced some alteration during the tectonic history of several orogenic events, but detailed studies of the organic matter thermal maturity in the Vinini Fm. suggest a relatively low grade thermal history (LaPorte et al., 2009; Poole and Claypool, 1984). Furthermore, ratios of $\text{Fe}_{\text{T}}/\text{Al}$ reveal constant Fe enrichment compared to average shale. Such enrichment suggests a generally high depositional influx of Fe decoupled from background detrital levels, which is unlikely to be caused by later stage diagenesis (Fig. 4D) (Reinhard et al., 2012). Thus, the Fe speciation measurements from core samples are likely reflecting past local water column anoxia that persisted during the Late Ordovician.

5.2. Paleo-basinal gradients in sediment- and water column chemistry

The multivariate analysis of the dataset from the Vinini Creek section indicates that mixing of detrital, organic and carbonate sedimentary components correlates with a large degree of the geochemical variance ($\sim 65\%$, Fig. 5). Hirnantian glacioeustasy may have driven temporal and spatial changes in these sedimentary components through the progradation of shallow-water facies. We can explore the expected effect on $\delta^{13}\text{C}_{\text{Org}}$ from mixing of two spatially separated organic matter reservoirs through the two-component end-member mixing model (Johnston et al., 2012). These hypothetical reservoirs may represent lateral points across a shelf-to-basin transect, where the shallow end-member is a carbonate platform with high amounts of carbonate, low concentrations of TOC, and enriched C isotopes values. The deep end-member is an outer shelf oxygen minimum zone with high concentrations of TOC, low carbonate content and relatively depleted C isotopic values. The mixing of these two end-members, with vastly different TOC contents, can lead to highly non-linear changes in the average C isotopic value of organic carbon, which matches the observations from the Vinini Creek section (Fig. 3A) (Johnston et al., 2012; Oehlert and Swart, 2014). The mixing model indicates that the Katian samples from the Vinini Creek section (and other sections, Fig. S7) are better approximated using a deep water end-member with $\delta^{13}\text{C}_{\text{Org}}$ of $\sim -31.19\%$, compared to a Hirnantian deep water end-member with $\delta^{13}\text{C}_{\text{Org}}$ of $\sim -29.76\%$. On the other hand, the difference between the Katian and Hirnantian shallow water end-members is much larger, at $\sim 3.13\%$ (-30.64% vs. -27.51% , Fig. 3A and 7B).

There are two main mechanisms that can drive gradients in $\delta^{13}\text{C}_{\text{Org}}$ from the shelf to deep basin: lateral changes in the taxonomic community (different isotopic fractionation during photosynthesis), or spatial differences in the local $\delta^{13}\text{C}_{\text{DIC}}$ of sea-water (Swart and Eberli, 2005; Patterson and Walter, 1994; Peterson et al., 2014). In the Vinini Creek section, a possible taxonomic shift

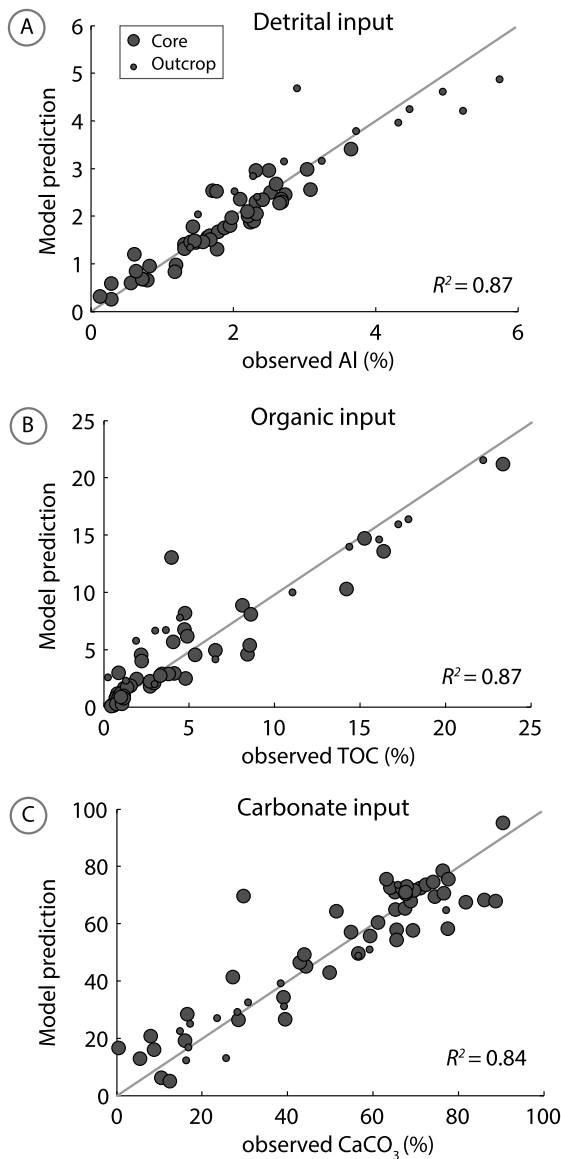


Fig. 6. Modeling the dataset in terms of three principal components using the reduced PCA model. **A.** The multivariate model prediction of the concentration of Al in comparison with observations. **B.** The multivariate model prediction of TOC. **C.** The multivariate model prediction of CaCO₃. The model predictions agree with the observed values with little unexplained variability (deviation from the 1:1 line indicated by R^2 value), suggesting that the sedimentary mixing of detrital, organic matter and carbonate input controls a large degree of the variance in the dataset.

has been recorded by organic biomarkers that indicate that organic matter in the Katian portion of the section is dominated by cyanobacterial sourced organic carbon whereas the Hirnantian portion of the section is dominated by algae (Rohrssen et al., 2013). Algae tend to have a larger fractionation factor than cyanobacteria and the inferred Hirnantian increase in algal communities would therefore be expected to cause an independent negative shift in $\delta^{13}\text{C}_{\text{Org}}$ (-2 – -1% , Hayes, 2001). However, the observed isotope excursion is positive, which suggests that the potential taxonomic effect was erased or modulated by more dominant mechanisms. Alternatively, spatial gradients in seawater $\delta^{13}\text{C}_{\text{DIC}}$ may be argued from the mixing relationship between $\delta^{13}\text{C}_{\text{Org}}$ and TOC. As such, the variation in sedimentary components does not directly cause the stratigraphic changes in $\delta^{13}\text{C}_{\text{Org}}$. Rather the variations in $\delta^{13}\text{C}_{\text{Org}}$ may in part be governed by spatial gradients in seawater $\delta^{13}\text{C}_{\text{DIC}}$, potentially amplified during the glaciation, and thus occurring in parallel with progradation of

shallow-water facies during the eustatic sea-level fall. Such gradients could explain the difference between the Katian and Hirnantian end-member mixing model and further substantiate the observed large range in $\delta^{13}\text{C}_{\text{Org}}$ and $\delta^{13}\text{C}_{\text{Carb}}$ across the Laurentian margin during the Hirnantian (Fig. 7) (Jones et al., in press; LaPorte et al., 2009).

Increased glacio-eustatic restriction of shallow epeiric seas may contribute to lateral gradients in $\delta^{13}\text{C}_{\text{DIC}}$ as platform water masses are progressively enriched in ^{13}C due to photosynthesis of the carbonate secreting organisms (Panchuk et al., 2005; Swart and Eberli, 2005). Additionally, vertical gradients in $\delta^{13}\text{C}_{\text{DIC}}$ may originate from the biological pump and the additional glacio-eustatic export of organic matter to the deeper basin as shelf areas decrease and rates of organic matter decomposition decline (Curry et al., 1988; Peterson et al., 2014). Glacioeustasy, therefore, may increase both lateral- and vertical gradient in $\delta^{13}\text{C}_{\text{DIC}}$ from the shallow shelf to the deep basin.

Spatial isotopic gradients can also be recorded in the stratigraphy of sulfur isotopes. Spatial differences in $\delta^{34}\text{S}_{\text{Py}}$ can be related to local sulfate reduction rates, the availability of reactive iron and sulfate, and the depth of the zone of sulfate reduction within the sediment column (e.g. Fike et al., 2015; Raiswell, 1982). Shallow sediments may be enriched in $\delta^{34}\text{S}_{\text{Py}}$ compared to deeper facies, due to partial oxidation of H_2S following sediment reworking or by limited exchange between pore-water and seawater sulfate due to rapid sedimentation rates (Fike et al., 2015; Fry et al., 1988; Raiswell, 1982). These effects may contribute to the positive $\delta^{34}\text{S}_{\text{Py}}$ excursion recorded in multiple sections across different paleo-continents during the Hirnantian glacio-eustatic sea-level fall (Hammarlund et al., 2012; Jones and Fike, 2013).

In contrast to the widespread observed positive excursion, $\delta^{34}\text{S}_{\text{Py}}$ in the Vinini Creek section is enriched in the deep Katian TOC rich facies, relative to the shallower Hirnantian periplatform facies (Fig. 3B). The observed exponential covariance between TOC and $\delta^{34}\text{S}_{\text{Py}}$ in the Vinini Creek section could indicate that isotopic fractionation was governed by local microbial sulfate reduction rates and the availability of electron donors such as organic matter (Leavitt et al., 2013; Sim et al., 2011). Higher sulfate reduction rates result in less fractionation between pore water sulfate and pyrite (Harrison and Thode, 1957). First order reaction kinetics may thus explain the general enrichment of $\delta^{34}\text{S}_{\text{Py}}$ in the high TOC Katian interval compared to the lighter $\delta^{34}\text{S}_{\text{Py}}$ values in the Hirnantian carbonates ($R^2 = 0.27$; Fig. 3B). Furthermore, the degree of scatter in the sulfur isotopic record from the Vinini Creek section is possibly linked to multiple generations of pyrite. Pyrite may be present as both framboidal pyrite, precipitating rapidly in the zone of sulphate reduction, and as euhedral pyrite forming within the sediment with near quantitative consumption of sulfate in closed system conditions (Raiswell, 1982; Magnall et al., 2016). Overall we conclude that most of the variability of $\delta^{34}\text{S}_{\text{Py}}$ in the Vinini Creek section likely reflects local redox conditions, either close to or below the sediment–water interface.

5.3. Secular changes in ocean chemistry across the Hirnantian

Multivariate statistical methods suggest that much of the geochemical variation in the Vinini Creek section correlates with mixing of sedimentary end-members and local spatial gradients in water column chemistry. However, geochemical trends that are decoupled from these local signals may be inferred from the unexplained components of the analysis (see Methods). Specifically, the cluster analysis indicates that variations in Fe speciation and TS are largely unrelated to variations in the major sedimentary components (Fig. 5C). These proxies are generally expected to respond to local redox conditions at or near the sediment water interface,

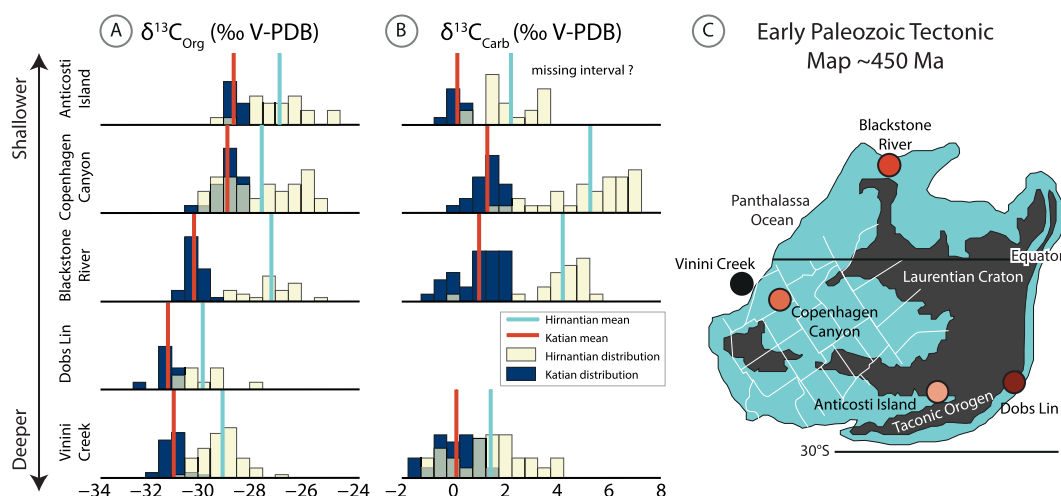


Fig. 7. Distribution of $\delta^{13}\text{C}_{\text{carb}}$ and $\delta^{13}\text{C}_{\text{org}}$ during the Late Ordovician (from Jones et al., 2011; LaPorte et al., 2009; Hammarlund et al., 2012). **A.** Histograms of the distribution of $\delta^{13}\text{C}_{\text{org}}$ from multiple sections across a range of paleo-water depths. The relative paleo-water depth is inferred from lithological interpretation (from Finney et al., 2007; LaPorte et al., 2009; Hammarlund et al., 2012; Jones et al., 2011, and references therein). **B.** Histograms of the distribution of $\delta^{13}\text{C}_{\text{carb}}$. It is worth noticing that missing intervals and the sampling density may contribute to differences in the distribution of these histograms but likely will not change the significant range in measurements. The Katian $\delta^{13}\text{C}_{\text{carb}}$ distribution from the Vinini Creek section is estimated from the *D. ornatus* interval in order to exclude possible diagenetic values (LaPorte et al., 2009). **C.** Early Paleozoic Tectonic Map indicating the approximate location of each section across the Laurentian margin. Late Ordovician paleogeography modified after (Blakey, 2013) (<http://cpgeosystems.com/namO485.jpg>).

but the cluster analysis demonstrates little relationship with other redox sensitive trace elements. While Fe speciation broadly tracks the euxinic–anoxic–oxic thresholds, it does not necessarily reflect the more detailed redox zones within anoxia (Raiswell and Canfield, 2012). Redox sensitive trace elements, on the other hand, are more sensitive to specific redox boundaries, and may have high affinities with organic matter accumulation (Tribouillard et al., 2006).

Sedimentary sulfur appears to predominantly occur in pyrite, as illustrated by a linear relationship between TS and Fe_{py} (Fig. S4). Constraints on pyrite formation may be inferred from the ratio of TS/TOC, where normal marine sedimentary ratios converge around 0.36 (Morse and Berner, 1995). Deviation from this normal ratio indicates limitations on microbial sulfate reduction and pyrite formation by insufficient labile organic carbon (high ratios) or reactive Fe and available sulfate (low ratios, Morse and Berner, 1995; Raiswell and Canfield, 2012). TS/TOC increases significantly across the Katian–Hirnantian boundary, which may reflect changes in pyrite formation and redox conditions during this interval (0.16 to 0.79, respectively; Fig. 3C). When considering the abundance of reactive Fe throughout the section ($\text{Fe}_{\text{HR}}/\text{Fe}_{\text{T}} > 0.38$), the low TS/TOC ratios in the Katian suggest that pyrite formation was limited by available pore water sulfate relative to organic carbon. In contrast, the high TS/TOC ratios in the Hirnantian may indicate a change in the limitations of pyrite formation. High ratios of TS/TOC are generally expected to correlate with a high degree of pyritization under euxinic conditions, but the ratios of $\text{Fe}_{\text{py}}/\text{Fe}_{\text{HR}}$ fall below the diagnostic euxinic threshold during this interval (Poulton and Canfield, 2011; Raiswell and Canfield, 2012). These observations may suggest that pyritization in the Vinini Fm. was instead limited by organic matter availability during the Hirnantian.

Changes in the processes controlling pyrite formation are possibly recorded in $\delta^{34}\text{S}_{\text{py}}$. Underlying trends in $\delta^{34}\text{S}_{\text{py}}$ that are independent of local sedimentary mixing may be inferred from the residual component of the reduced PCA model (see Methods). The structure of the residual component can be visualized by plotting model predictions against observed data and inspecting the deviation from the 1:1 identity relationship (Fig. 8). The residual component of $\delta^{34}\text{S}_{\text{py}}$ is structured towards the more depleted Hirnantian isotopic values where the model mostly over estimates. This residual depletion in $\delta^{34}\text{S}_{\text{py}}$ in the Hirnantian samples may

be tied to the Hirnantian shift in TS/TOC, and is consistent with larger isotopic fractionation caused by decreasing microbial sulfate reduction rates limited by organic matter availability (Leavitt et al., 2013; Sim et al., 2011). Furthermore, redox sensitive trace elements such as V, U, Zn and Mo, that may distinguish specific redox conditions, are strongly associated with organic matter variability in the Vinini Creek section and are generally well captured by the reduced PCA model (Figs. 5 and S7) (Tribouillard et al., 2006). This relationship suggests that local organic matter availability controlled both sulfate reduction rates and redox conditions during the latest Ordovician.

Trends in $\delta^{13}\text{C}_{\text{org}}$ that are decoupled from both local sedimentary mixing and lateral gradients in water column $\delta^{13}\text{C}_{\text{DIC}}$ may be inferred from the unexplained components of the reduced PCA analysis. The goodness of fit of the model ($R^2 = 0.72$, Fig. 8A) substantiates the first order spatial and local control on $\delta^{13}\text{C}_{\text{org}}$. However, whereas the Katian samples broadly fit the reduced PCA model, the residual of the model demonstrates that the absolute $\delta^{13}\text{C}_{\text{org}}$ values are consistently under estimated during the Hirnantian, by an offset of $\sim 1\text{‰}$ (Fig. 8A). It has previously been recognized that the open oceans experienced a smaller $\delta^{13}\text{C}_{\text{DIC}}$ shift than the epeiric seas during the Hirnantian period (e.g. Jones et al., 2011, in press; LaPorte et al., 2009; Panchuk et al., 2005). These considerations make it difficult to estimate the absolute magnitude of the secular change in $\delta^{13}\text{C}_{\text{DIC}}$ related to the Hirnantian glaciation. Shallow carbonate platform environments dominate the Hirnantian stratigraphy, recording up to $+7\text{‰}$ apparent perturbation in $\delta^{13}\text{C}_{\text{carb}}$. In contrast, deeper water environments, similar to the Vinini Creek section, record a substantially smaller positive excursion $\sim +1\text{--}3\text{‰}$ in both $\delta^{13}\text{C}_{\text{carb}}$ and $\delta^{13}\text{C}_{\text{org}}$ (Kump et al., 1999) (Fig. 7).

Taken at face value, our multivariate analysis leads us to speculate that the open ocean Hirnantian carbon isotope excursion may amount to only $\sim +1.5\text{‰}$ $\delta^{13}\text{C}_{\text{DIC}}$, with the remainder of the observed excursion caused by local amplification in shallower carbonate platform environments driven by glacio-eustasy. This open ocean estimate is based on the reduced PCA model, which indicates a $+1\text{‰}$ residual in $\delta^{13}\text{C}_{\text{org}}$ in Hirnantian samples that can be interpreted as a minimum estimate of the open ocean isotope excursion isolated from local effects of sediment mixing and lateral gradients in water column chemistry (Fig. 8A). The two compo-

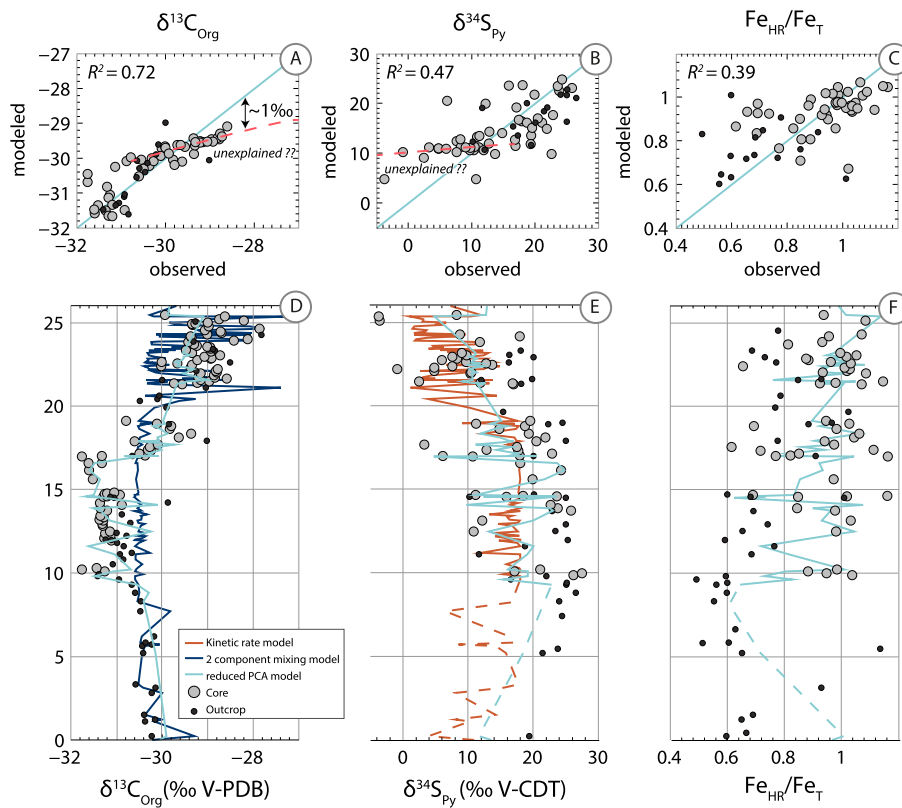


Fig. 8. Comparison between modeled and observed geochemical variability. **A.** The reduced PCA model captures much of the observed variability in $\delta^{13}\text{C}_{\text{Org}}$ but with a residual component in heavier values of up to $\sim 1\text{‰}$ (deviation from the 1:1 identity line). **B.** Model predictions of $\delta^{34}\text{S}_{\text{Py}}$ show some degree of unexplained variance, especially below 10‰ where the model over predicts the isotopic value. **C.** $\text{Fe}_{\text{HR}}/\text{Fe}_{\text{T}}$ demonstrates little correlation with the model prediction, indicating that sediment mixing was not a strong control on Fe speciation. **D.** Stratigraphic expression of $\delta^{13}\text{C}_{\text{Org}}$ in comparison with both the reduced PCA model and the simple two component end-member mixing model. **E.** Stratigraphic comparison between observed $\delta^{34}\text{S}_{\text{Py}}$ and both the reduced PCA and the first order kinetic rate model. **F.** Stratigraphic variability of $\text{Fe}_{\text{HR}}/\text{Fe}_{\text{T}}$ in comparison with the reduced PCA model.

ment mixing model further supports this estimate, and indicates a $+1.4\text{‰}$ shift in $\delta^{13}\text{C}_{\text{Org}}$ between the deep-water Katian and Hirnantian end-members (Fig. 3A). Furthermore, extending the mixing model to include other Laurentian sections consistently shows a difference between the relative deep-water Katian and Hirnantian end-members of approximately $+1.6\text{‰}$, which may be interpreted to reflect a change in open ocean $\delta^{13}\text{C}_{\text{DIC}}$ (Fig. S7). The speculation of a $+1.5\text{‰}$ secular open ocean excursion in $\delta^{13}\text{C}_{\text{DIC}}$ requires a constant photosynthetic isotope fractionation between $\delta^{13}\text{C}_{\text{Org}}$ and $\delta^{13}\text{C}_{\text{Carb}}$, as demonstrated in multiple Hirnantian sections (Jones et al., 2011; Panchuk et al., 2005).

A positive excursion is traditionally modeled by a relative increase in organic carbon burial, f_{Org} (the fraction of organic carbon relative to total carbon burial; Kump and Arthur, 1999). Carbonate carbon burial, at this time, was predominantly constrained by platform areas due to the lack of a significant deep-sea sedimentary carbonate sink (Ridgwell and Zeebe, 2005). We take this into account and approximate f_{Org} by splitting the carbonate burial sink into a platform sink ($80\% \pm 20\% 2\sigma$) and a deep pelagic sink ($20\% \pm 20\% 2\sigma$) with a conservative constant isotopic enrichment of $+2\text{‰}$ in platform $\delta^{13}\text{C}_{\text{DIC}}$ relative to the open ocean (cf. Fig. 7 and supplementary information, Bjerrum and Canfield, 2004; Ridgwell and Zeebe, 2005). As such, a steady state $+1.5\text{‰}$ excursion in $\delta^{13}\text{C}_{\text{DIC}}$ from the Katian to the Hirnantian would amount to $\sim 19\%$ increase in f_{Org} ($\pm 3.9\% 2\sigma$, Monte Carlo error propagation). This relatively small increase could be directly driven through glacioeustasy by shifting organic matter export towards the deep ocean, as is observed during the Pleistocene (Curry et al., 1988; Jaccard et al., 2009). The lateral shift in organic matter remineralization would push oxygen demand towards the deep ocean

where oxygen levels were likely already low (Hammarlund et al., 2012; Sperling et al., 2015). Low oxygen levels are consistent with Fe speciation measurements from the Vinini Creek section that demonstrate persistent local anoxic conditions throughout the late Ordovician independent of glacioeustasy. The combination of deep water anoxia and cooler glacial temperatures would increase the organic carbon burial efficiency over the large deep marine seafloor area (Finnegan et al., 2012). Together, we argue that these mechanisms facilitated an increase in f_{Org} and thus provide a causal relationship between the positive excursion in $\delta^{13}\text{C}_{\text{DIC}}$ and the Hirnantian glaciation.

6. Conclusion

The Vinini Creek section in central Nevada provides a unique deep basinal perspective on a sedimentary record dominated by widespread shallow water carbonate deposits. Despite the Hirnantian glacio-eustatic sea-level fall, new evidence from $\text{Fe}_{\text{HR}}/\text{Fe}_{\text{T}}$ in shallow drill-core samples indicates that the deep water column remained anoxic throughout the latest Ordovician, in contrast to observations from sections deposited at shallower water depths (Melchin et al., 2013). In comparison with drill-core samples, measurements from outcrop demonstrate that modern weathering clearly alters pyrite concentrations, which affects ratios of $\text{Fe}_{\text{Py}}/\text{Fe}_{\text{HR}}$, $\text{Fe}_{\text{HR}}/\text{Fe}_{\text{T}}$ and potentially $\delta^{34}\text{S}_{\text{Py}}$.

Multivariate statistical methods indicate that mixing of detrital material, organic matter, and carbonate strongly correlates with the geochemical variation in the Vinini Creek section. Glacioeustasy drove progradation of local sedimentary environments and increased lateral- and vertical gradients in seawater

redox chemistry from the shallow shelf to the deep ocean. Such spatial gradients were amplified by both glacio-eustatic restriction of shallow water environments and increased transfer of organic matter to the deep basin. These prevailing local effects are recorded as non-linear end-member mixing between $\delta^{13}\text{C}_{\text{Org}}$ and TOC. This trend that is also recorded in $\delta^{34}\text{S}_{\text{Py}}$, as sulfate reduction rates were limited by the local availability of labile organic matter.

In addition to changing local environments, glacioeustasy may have driven global changes in ocean chemistry. We attempt to isolate these secular changes using a two component mixing model and residuals from a reduced PCA model that captures the control of local sedimentary processes and spatial gradients in seawater chemistry. This approach results in an estimated global average perturbation of $\sim +1.5\text{‰}$ in $\delta^{13}\text{C}_{\text{DIC}}$ during the Hirnantian, significantly less than the up to $\sim +7\text{‰}$ perturbation estimated by previous studies (Kump et al., 1999). Such a relatively small increase in $\delta^{13}\text{C}_{\text{DIC}}$ could be caused by a transfer of organic matter export to the anoxic basin, which increased the organic carbon burial efficiency over the large deep seafloor area. This approach illustrates the applicability of multivariate statistical methods in disentangling past environmental signals, and highlights the need to consider combined local and global changes in seawater chemistry when interpreting ancient stratigraphy.

Acknowledgements

We would like to thank Benjamin Gill, Erik Sperling, and one anonymous reviewer for careful, constructive, and concrete reviews that greatly improved the manuscript. We would also like to thank our field assistants S. LaFontaine, D. Mills, S. Rosing, M. Ruhl, and F. S nderholm for numerous hours of drilling in Vinini Creek and V. Moser, H. Jensen, and S. M ller for assistance in the lab. We are grateful for inspiring conversations and helpful comments on the manuscript by B. Dyer, M. Lenniger, and T. Dahl. The authors were supported by the Danish National Research Foundation (grant no. DNRF53). CJB acknowledges support for drill equipment from Maersk Oil and Gas, Carlsberg Foundation (grant no. 2011-01-0705), and Danish Council for Independent Research (0602-00602B).

Appendix A. Supplementary material

Supplementary material related to this article can be found online at <http://dx.doi.org/10.1016/j.epsl.2016.09.049>.

References

- Berry, W.B.N., Boucot, A.J., 1973. Glacio-eustatic control of Late Ordovician-Early Silurian platform sedimentation and faunal changes. *Geol. Soc. Am. Bull.* 84 (1), 275–284. [http://dx.doi.org/10.1130/0016-7606\(1973\)84<275:gcolos>2.0.co;2](http://dx.doi.org/10.1130/0016-7606(1973)84<275:gcolos>2.0.co;2).
- Bjerrum, C.J., Bendtsen, J., Legarth, J.J.F., 2006. Modeling organic carbon burial during sea level rise with reference to the Cretaceous. *Geochem. Geophys. Geosyst.* 7 (5), 1–24. <http://dx.doi.org/10.1029/2005GC001032>.
- Bjerrum, C.J., Canfield, D.E., 2004. New insights into the burial history of organic carbon on the early Earth. *Geochem. Geophys. Geosyst.* 5 (8), 1–9. <http://dx.doi.org/10.1029/2004GC000713>.
- Blakey, R., 2013. Home paleogeographic maps products publications. Colorado Plateau Geosystems Online Database, <http://cpgeosystems.com/nam0485.jpg>.
- Brenchley, P.J., Marshal, J.D., Carden, G.A.F., Robertson, D.B.R., Long, D.G.F., Meidla, T., Hints, L., Anderson, T.F., 1994. Bathymetric and isotopic evidence for a short-lived Late Ordovician glaciation in a greenhouse period. *Geology* 22, 295–298. [http://dx.doi.org/10.1130/0091-7613\(1994\)022<0295:BAIEFA>2.3.CO;2](http://dx.doi.org/10.1130/0091-7613(1994)022<0295:BAIEFA>2.3.CO;2).
- Canfield, D.E., Poulton, S.W., Knoll, A.H., Narbonne, G.M., Ross, G., Goldberg, T., Strauss, H., 2008. Ferruginous conditions dominated later Neoproterozoic deep-water chemistry. *Science* 321 (5891), 949–952. <http://dx.doi.org/10.1126/science.1154499>.
- Canfield, D.E., Raiswell, R., Westrich, J.T., Reaves, C.M., Berner, R.A., 1986. The use of chromium reduction in the analysis of reduced inorganic sulfur in sediments and shales. *Chem. Geol.* 54, 149–155. [http://dx.doi.org/10.1016/0009-2541\(86\)90078-1](http://dx.doi.org/10.1016/0009-2541(86)90078-1).
- Cartapanis, O., Bianchi, D., Jaccard, S.L., Galbraith, E.D., 2016. Global pulses of organic carbon burial in deep-sea sediments during glacial maxima. *Nat. Commun.* 7. <http://dx.doi.org/10.1038/ncomms10796>.
- Clarkson, M.O., Poulton, S.W., Guilbaud, R., Wood, R.A., 2014. Assessing the utility of Fe/Al and Fe-speciation to record water column redox conditions in carbonate-rich sediments. *Chem. Geol.* 382, 111–122. <http://dx.doi.org/10.1016/j.chemgeo.2013.05.031>.
- Curry, W.B., Duplessy, J.C., Labeyrie, L.D., Shackleton, N.J., 1988. Changes in the distribution of $\delta^{13}\text{C}$ of deep water ΣCO_2 between the last glaciation and the holocene. *Paleoceanography* 3 (3), 317–341. <http://dx.doi.org/10.1029/PA003i003p00317>.
- Curtis, C.D., Murchison, D.G., Berner, R.A., Shaw, H., Sarntheim, M., Durand, B., Eglinton, G., Mackenzie, A.S., Surdam, R.C., 1985. Clay mineral precipitation and transformation during burial diagenesis. *Philos. Trans. R. Soc. Lond. A, Math. Phys. Eng. Sci.* 315 (1531), 91–105. <http://dx.doi.org/10.1098/rsta.1985.0031>.
- Dahl, T.W., Ruhl, M., Hammarlund, E.U., Canfield, D.E., Rosing, M.T., Bjerrum, C.J., 2013. Tracing euxinia by molybdenum concentrations in sediments using handheld X-ray fluorescence spectroscopy (HH-XRF). *Chem. Geol.* 360–361, 241–251. <http://dx.doi.org/10.1016/j.chemgeo.2013.10.022>.
- Fike, D.A., Bradley, A.S., Rose, C.V., 2015. Rethinking the ancient sulfur cycle. *Annu. Rev. Earth Planet. Sci.* 43 (1), 593–622. <http://dx.doi.org/10.1146/annurev-earth-060313-054802>.
- Finnegan, S., Fike, D.A., Jones, D., Fischer, W.W., 2012. A temperature-dependent positive feedback on the magnitude of carbon isotope excursions. *Geosci. Can. (ISSN 1911-4850)* 39 (3).
- Finney, S.C., Berry, W.B.N., Cooper, J.D., 2007. The influence of denitrifying seawater on graptolite extinction and diversification during the Hirnantian (latest Ordovician) mass extinction event. *Lethaia* 40, 281–291. <http://dx.doi.org/10.1111/j.1502-3931.2007.00027.x>.
- Finney, S.C., Berry, W.B.N., Cooper, J.D., Ripperdan, R.L., Sweet, W.C., Jacobson, S.R., Soufiane, A., Achab, A., Noble, P.J., 1999. Late Ordovician mass extinction: a new perspective from stratigraphic sections in central Nevada. *Geology* 27, 215–218. [http://dx.doi.org/10.1130/0091-7613\(1999\)027<0215:LOMEAN>2.3.CO;2](http://dx.doi.org/10.1130/0091-7613(1999)027<0215:LOMEAN>2.3.CO;2).
- Finney, S.C., Cooper, J.D., Berry, W.B.N., 1998. Late Ordovician mass extinction: sedimentologic, cyclostratigraphic, and biostratigraphic records from platform and basin successions, central Nevada. *BYU Geol. Stud.* 42 (1), 79–103.
- Finney, S.C., Noble, P.J., Cluer, J.K., 2000. Lower Paleozoic stratigraphy and structure of central Nevada: comparisons and contrasts between the lower and upper plates of the Roberts Mountains thrust. In: *GSA Field Guides*, vol. 2, pp. 279–300. <http://dx.doi.org/10.1130/0-8137-0002-7.279>.
- Fry, B., Ruf, W., Gest, H., Hayes, J.M., 1988. Sulfur isotope effects associated with oxidation of sulfide by O_2 in aqueous solution. *Chem. Geol., Isot. Geosci. Sect.* 73 (3), 205–210. [http://dx.doi.org/10.1016/0168-9622\(88\)90001-2](http://dx.doi.org/10.1016/0168-9622(88)90001-2).
- Ghienne, J.-F., Desrochers, A., Vandenbroucke, T.R.A., Achab, A., Asselin, E., Dabard, M.-P., Farley, C., Loi, A., Paris, F., Wickson, S., Veizer, J., 2014. A Cenozoic-style scenario for the end-Ordovician glaciation. *Nat. Commun.* 5 (4485).
- Hammarlund, E.U., Dahl, T.W., Harper, D.A.T., Bond, D.P.G., Nielsen, A.T., Bjerrum, C.J., Schovsbo, N.H., Sch nlaub, H.P., Zalasiewicz, J.A., Canfield, D.E., 2012. A sulfidic driver for the end-Ordovician mass extinction. *Earth Planet. Sci. Lett.* 331–332, 128–139. <http://dx.doi.org/10.1016/j.epsl.2012.02.024>.
- Hammer,  ., Harper, D.A.T., 2006. *Paleontological Data Analysis*. Blackwell Publishing, 351 pp. <http://dx.doi.org/10.1002/9780470750711>.
- Harrison, A.G., Thode, H.G., 1957. The kinetic isotope effect in the chemical reduction of sulphate. *Trans. Faraday Soc.* 53, 1648–1651. <http://dx.doi.org/10.1039/TF9575301648>.
- Hayes, J.M., 2001. Fractionation of carbon and hydrogen isotopes in biosynthetic processes. *Rev. Mineral. Geochem.* 43 (1), 225–277. <http://dx.doi.org/10.2138/gsrmg.43.1.225>.
- Holmden, C., Mitchell, C.E., LaPorte, D.F., Patterson, W.P., Melchin, M.J., Finney, S.C., 2013. Nd isotope records of late Ordovician sea-level change—implications for glaciation frequency and global stratigraphic correlation. *Palaeogeogr. Palaeoclimatol. Palaeoecol.* 386, 131–144.
- Jaccard, S.L., Galbraith, E.D., 2012. Large climate-driven changes of oceanic oxygen concentrations during the last deglaciation. *Nat. Geosci.* 5 (2), 151–156. <http://dx.doi.org/10.1038/ngeo1352>. <http://www.nature.com/ngeo/journal/v5/n2/abs/ngeo1352.html/supplementary-information>.
- Jaccard, S.L., Galbraith, E.D., Sigman, D.M., Haug, G.H., Francois, R., Pedersen, T.F., Dulski, P., Thierstein, H.R., 2009. Subarctic pacific evidence for a glacial deepening of the oceanic respired carbon pool. *Earth Planet. Sci. Lett.* 277 (1–2), 156–165. <http://dx.doi.org/10.1016/j.epsl.2008.10.017>.
- Johnston, D.T., Macdonald, F.A., Gill, B.C., Hoffman, P.F., Schrag, D.P., 2012. Uncovering the Neoproterozoic carbon cycle. *Nature* 483 (7389), 320–323. <http://dx.doi.org/10.1038/nature10854>.
- Jones, D.S., Creel, R.C., Rios, B.A., in press. Carbon isotope stratigraphy and correlation of depositional sequences in the Upper Ordovician Ely Springs Dolostone, Eastern Great Basin, USA. *Palaeogeogr. Palaeoclimatol. Palaeoecol.* <http://dx.doi.org/10.1016/j.palaeo.2016.01.036>.
- Jones, D.S., Fike, D.A., 2013. Dynamic sulfur and carbon cycling through the end-Ordovician extinction revealed by paired sulfate-pyrite $\delta^{34}\text{S}$. *Earth Planet. Sci. Lett.* 363, 144–155. <http://dx.doi.org/10.1016/j.epsl.2012.12.015>.

- Jones, D.S., Fike, D.A., Finnegan, S., Fischer, W.W., Schrag, D.P., McCay, D., 2011. Terminal Ordovician carbon isotope stratigraphy and glacioeustatic sea-level change across Anticosti Island (Québec, Canada). *Geology* 123 (7–8), 1645–1664. <http://dx.doi.org/10.1130/B30323.1>.
- Kump, L.R., Arthur, M.A., 1999. Interpreting carbon-isotope excursions: carbonates and organic matter. *Chem. Geol.* 161 (1–3), 181–198. [http://dx.doi.org/10.1016/S0009-2541\(99\)00086-8](http://dx.doi.org/10.1016/S0009-2541(99)00086-8).
- Kump, L.R., Arthur, M.A., Patzkowsky, M.E., Gibbs, M.T., Pinkus, D.S., Sheehan, P.M., 1999. A weathering hypothesis for glaciation at high atmospheric pCO₂ during the Late Ordovician. *Palaeogeogr. Palaeoclimatol.* 152, 173–187. [http://dx.doi.org/10.1016/S0031-0182\(99\)00046-2](http://dx.doi.org/10.1016/S0031-0182(99)00046-2).
- LaPorte, D.F., Holmden, C., Patterson, W.P., Loxton, J.D., Melchin, M.J., Mitchell, C.E., Finney, S.C., Sheets, H.D., 2009. Local and global perspectives on carbon and nitrogen cycling during the Hirnantian glaciation. *Palaeogeogr. Palaeoclimatol. Palaeoecol.* 276, 182–195. <http://dx.doi.org/10.1016/j.palaeo.2009.03.009>.
- Leavitt, D.L., Halevy, I., Bradley, A.S., Johnston, D.T., 2013. Influence of sulfate reduction rates on the Phanerozoic sulfur isotope record. *Proc. Natl. Acad. Sci.* 110 (28), 11244–11249. <http://dx.doi.org/10.1073/pnas.1218874110>.
- Lenton, T.M., Crouch, M., Johnson, M., Pires, N., Dolan, L., 2012. First plants cooled the Ordovician. *Nat. Geosci.* 5 (2), 86–89. <http://dx.doi.org/10.1038/ngeo1390>.
- Magnall, J.M., Gleeson, S.A., Stern, R.A., Newton, R.J., Poulton, S.W., Paradis, S., 2016. Open system sulphate reduction in a diagenetic environment— isotopic analysis of barite ($\delta^{34}\text{S}$ and $\delta^{18}\text{O}$) and pyrite ($\delta^{34}\text{S}$) from the Tom and Jason Late Devonian Zn–Pb–Ba deposits, Selwyn Basin, Canada. *Geochim. Cosmochim. Acta* 180, 146–163. <http://dx.doi.org/10.1016/j.gca.2016.02.015>.
- Marden, J.J., 2015. *Multivariate Statistics: Old School*. CreateSpace Independent Publishing Platform, ISBN 978-1456538835.
- Melchin, M.J., Mitchell, C.E., Holmden, C., Storch, P., 2013. Environmental changes in the Late Ordovician-early Silurian: review and new insights from black shales and nitrogen isotopes. *Geol. Soc. Am. Bull.* 125 (11/12), 1635–1670. <http://dx.doi.org/10.1130/B30812.1>.
- Merriam, C.W., Anderson, C.A., 1942. Reconnaissance survey of the Roberts Mountains, Nevada. *Geol. Soc. Am. Bull.* 53, 1675–1728.
- Morse, J.W., Berner, R.A., 1995. What determines sedimentary C/S ratios? *Geochim. Cosmochim. Acta* 59 (6), 1073–1077. [http://dx.doi.org/10.1016/0016-7037\(95\)00024-T](http://dx.doi.org/10.1016/0016-7037(95)00024-T).
- Oehlert, A.M., Swart, P.K., 2014. Interpreting carbonate and organic carbon isotope covariance in the sedimentary record. *Nat. Commun.* 5. <http://dx.doi.org/10.1038/ncomms5672>.
- Panchuk, K.M., Holmden, C., Kump, L.R., 2005. Sensitivity of the epeiric sea carbon isotope record to local-scale carbon cycle processes: tales from the Mohawkian Sea. *Palaeogeogr. Palaeoclimatol. Palaeoecol.* 228 (3–4), 320–337. <http://dx.doi.org/10.1016/j.palaeo.2005.06.019>.
- Patterson, W.P., Walter, L.M., 1994. Depletion of ^{13}C in seawater ΣCO_2 on modern carbonate platforms: significance for the carbon isotopic record of carbonates. *Geology* 22 (10), 885–888. [http://dx.doi.org/10.1130/0091-7613\(1994\)022<0885:docisc>2.3.co;2](http://dx.doi.org/10.1130/0091-7613(1994)022<0885:docisc>2.3.co;2).
- Perkins, R.B., Mason, C.E., 2015. The relative mobility of trace elements from short-term weathering of a black shale. *Appl. Geochem.* 56, 67–79. <http://dx.doi.org/10.1016/j.apgeochem.2015.01.014>.
- Peterson, C.D., Lisiecki, L.E., Stern, J.V., 2014. Deglacial whole-ocean $\delta^{13}\text{C}$ change estimated from 480 benthic foraminiferal records. *Paleoceanography* 29 (6), 549–563. <http://dx.doi.org/10.1002/2013PA002552>.
- Petsch, S.T., Berner, R.A., Eglinton, T.I., 2000. A field study of the chemical weathering of ancient sedimentary organic matter. *Org. Geochem.* 31 (5), 475–487. [http://dx.doi.org/10.1016/S0146-6380\(00\)00014-0](http://dx.doi.org/10.1016/S0146-6380(00)00014-0).
- Poole, F.G., Claypool, G.E., 1984. Petroleum source-rock potential and crude-oil correlation in the great basin. In: Woodward, J., Meissner, F.F., Clayton, J.L. (Eds.), *Hydrocarbon Source Rocks of the Greater Rocky Mountain Region*. Rocky Mountain Association of Geologists, pp. 179–229.
- Poulton, S.W., Canfield, D., 2011. Ferruginous conditions: a dominant feature of the ocean through Earth's history. *Elements* 7, 107–112. <http://dx.doi.org/10.2113/gselements.7.2.107>.
- Poulton, S.W., Canfield, D.E., 2005. Development of a sequential extraction procedure for iron: implications for iron partitioning in continentally derived particulates. *Chem. Geol.* 214, 209–221. <http://dx.doi.org/10.1016/j.chemgeo.2004.09.003>.
- Raiswell, R., 1982. Pyrite texture, isotopic composition and the availability of iron. *Am. J. Sci.* 282 (8), 1244–1263. <http://dx.doi.org/10.2475/ajs.282.8.1244>.
- Raiswell, R., Canfield, D.E., 2012. The iron biogeochemical cycle past and present. *Geochem. Perspect.* 1 (1), 1–2. <http://dx.doi.org/10.7185/geochempersp.1.1>.
- Raup, D.M., Sepkoski, J.J., 1982. Mass extinctions in the marine fossil record. *Science* 215 (4539), 1501–1503. <http://dx.doi.org/10.1126/science.215.4539.1501>.
- Reinhard, C.T., Lyons, T.W., Rouxel, O., Asael, D., Dauphas, N., Kump, L.R., 2012. Iron speciation and isotope perspectives on Palaeoproterozoic water column chemistry. In: *Drilling Early Earth Project*, vol. 3. Springer-Verlag, Berlin, Heidelberg, pp. 1483–1492, book section 7.10.4.
- Ridgwell, A., Zeebe, R.E., 2005. The role of the global carbonate cycle in the regulation and evolution of the Earth system. *Earth Planet. Sci. Lett.* 234 (3–4), 299–315. <http://dx.doi.org/10.1016/j.epsl.2005.03.006>.
- Rohrsen, M., Love, G.D., Fischer, W.W., Finnegan, S., Fike, D.A., 2013. Lipid biomarkers record fundamental changes in the microbial community structure of tropical seas during the Late Ordovician Hirnantian glaciation. *Geology* 41 (2), 127–130. <http://dx.doi.org/10.1130/G33671.1>.
- Sheets, H.D., Mitchell, C.E., Melchin, M.J., Loxton, J., Štorch, P., Carlucci, K.L., Hawkins, A.D., 2016. Graptolite community responses to global climate change and the Late Ordovician mass extinction. *Proc. Nat. Acad. Sci.* 113 (30), 8380–8385.
- Sim, M.S., Ono, S., Donovan, K., Templer, S.P., Bosak, T., 2011. Effect of electron donors on the fractionation of sulfur isotopes by a marine *Desulfovibrio* sp. *Geochim. Cosmochim. Acta* 75 (15), 4244–4259. <http://dx.doi.org/10.1016/j.gca.2011.05.021>.
- Southam, J.R., Hay, W.W., 1977. Time scales and dynamic models of deep-sea sedimentation. *J. Geophys. Res.* 82 (27), 3825–3842. <http://dx.doi.org/10.1029/JC082i027p03825>.
- Sperling, E.A., Wolock, C.J., Morgan, A.S., Gill, B.C., Kunzmann, M., Halverson, G.P., Macdonald, F.A., Knoll, A.H., Johnston, D.T., 2015. Statistical analysis of iron geochemical data suggests limited Late Proterozoic oxygenation. *Nature* 523 (7561), 451–454. <http://dx.doi.org/10.1038/nature14589>.
- Swart, P.K., Eberli, G., 2005. The nature of the $\delta^{13}\text{C}$ of periplatform sediments: implications for stratigraphy and the global carbon cycle. *Sediment. Geol.* 175 (1–4), 115–129. <http://dx.doi.org/10.1016/j.sedgeo.2004.12.029>.
- Tribouillard, N., Algeo, T.J., Lyons, T.W., Riboulleau, A., 2006. Trace metals as paleoredox and paleoproductivity proxies: an update. *Chem. Geol.* 232, 12–32. <http://dx.doi.org/10.1016/j.chemgeo.2006.02.012>.
- Wedepohl, K.H., 1971. Environmental influences on the chemical composition of shales and clays. *Phys. Chem. Earth* 8, 305–333. [http://dx.doi.org/10.1016/0079-1946\(71\)90020-6](http://dx.doi.org/10.1016/0079-1946(71)90020-6).